



Extrinsic spin-valley Hall effect and spin-relaxation anisotropy in magnetized and strained grapheneXian-Peng Zhang *Donostia International Physics Center, Manuel de Lardizabal, 4. 20018, San Sebastian, Spain
and Department of Physics, University of Basel, Klingelbergstrasse 82, 4056 Basel, Switzerland* (Received 1 July 2022; revised 1 September 2022; accepted 6 September 2022; published 27 September 2022)

The implementation of the quantum spin-valley Hall effect is a critical challenge for the spintronics and valleytronic experimentalists because it requires breaking both time-reversal symmetry (\mathcal{T}) and spatial inversion symmetry (\mathcal{P}) while preserving the joint symmetry $\mathcal{O} = \mathcal{TP}$. Here, we demonstrate an extrinsic spin-valley Hall effect by the magnetic field and temperature modulation of the nonlocal resistance in a Hall bar device consisting of magnetized and strained graphene. Besides, we achieve a striking crossover from positive to negative nonlocal magnetoresistance owing to the magnetic field dependence of spin-valley relaxation instead of the usual Hanle spin precession. Moreover, we microscopically derive a large and tunable spin-relaxation anisotropy of the magnetized graphene within the Born-Markov and the Weiss-field approximations. Our findings offer fascinating opportunities to manipulate the spin and valley degrees of freedom and design novel electronic devices.

DOI: [10.1103/PhysRevB.106.115437](https://doi.org/10.1103/PhysRevB.106.115437)**I. INTRODUCTION**

The discovery of a large magnetic exchange field in two-dimensional (2D) materials/ferromagnetic insulator heterostructures has spurred a resurgence of interest in spintronics [1–9] that enables local spin manipulation via magnetic gates [10,11] and efficient spin generation for spintronic applications [12,13]. The 2D materials without intrinsic magnetism, such as graphene [4–7] and monolayer transition-metal dichalcogenides [8,9], are supposed to have a large interfacial magnetic exchange field owing to the short-range nature of the ferromagnetic proximity effect [14]. Ferromagnetic insulator EuS induces a large magnetic exchange field (>10 Tesla) in the graphene/EuS [1] and WSe₂ monolayer/EuS [2] heterostructures with the potential to reach hundreds of Tesla. Furthermore, first-principles calculations have demonstrated a magnetic exchange field in functionalized bismuth monolayers with strong spin-orbit coupling [15], where LaFeO₃ magnetic substrates introduce a staggered exchange field to break both time-reversal (\mathcal{T}) and spatial inversion (\mathcal{P}) symmetries, with the latter resulting in quantum valley Hall effect [16–18]. Thus, we reach the coexistence of quantum spin and valley Hall effects. The integration of spin and valley transport is ubiquitous in 2D materials with broken \mathcal{T} and/or \mathcal{P} symmetry [15,19–23], which provides eye-catching opportunities for novel electronic devices, such as spin-valley filters [24–26] and valley-spin valves [27,28].

Moreover, the combination of the spin and valley degrees of freedom offers fascinating opportunities to achieve an exotic transport phenomenon: quantum spin-valley Hall effect (SVHE) [29–34]. However, it is a critical challenge for spintronics and valleytronics experimentalists to implement quantum SVHE because it requires breaking both the \mathcal{T} and the \mathcal{P} symmetries while preserving the joint

symmetry $\mathcal{O} = \mathcal{TP}$ [19,20,32]. Consequently, there are few experimentally feasible proposals for quantum SVHE in condensate matter systems, such as antiferromagnetic manganese chalcogenophosphates [20], strained graphene [30], SbAsH₂ [33] monolayer, side-potential graphene [34], AA-stacked graphene bilayer [35], and graphene monolayer with an in-plane applied magnetic field [36]. Alternatively, an optically reconfigurable quantum SVHE was recently proposed in a 2D honeycomb array of ring resonators [32]. So far, most proposals are in the quantum regime, while little attention is paid to the classical version of the SVHE.

In this work, we present an experimentally feasible proposal for the classical SVHE in strained and magnetized graphene. Graphene subject to modest strain levels can sustain valley Hall current as a result of breaking \mathcal{P} symmetry [37]. Besides, if the \mathcal{T} -broken magnetic atoms induce local magnetized coupling [5,6], such functionalized graphene can generate a longitudinal spin current as well. The interplay of the transverse valley and longitudinal spin currents leads to the emergence of an additional transverse neutral spin-valley current. The existence of SVHE can be proved by the presence of out-of-plane magnetic field and temperature dependence of nonlocal resistance, which results from the magnetic field and temperature dependence of the spin-valley Hall angle and diffusion length. Furthermore, we microscopically derive a large and tunable spin-relaxation anisotropy of the magnetized graphene within the Born-Markov and the Weiss-field approximations.

We organize the remainder of this paper as follows. In Sec. II, we describe the detailed Hamiltonian of the hybrid itinerant electron and magnetic moment system. In Sec. III, we present the microscopic theory of the spin anisotropy and the extrinsic spin-valley Hall effect in the strained and magnetized graphene. In Sec. IV, we take ferromagnetic insulator EuS as an example and show our main results and discussions.

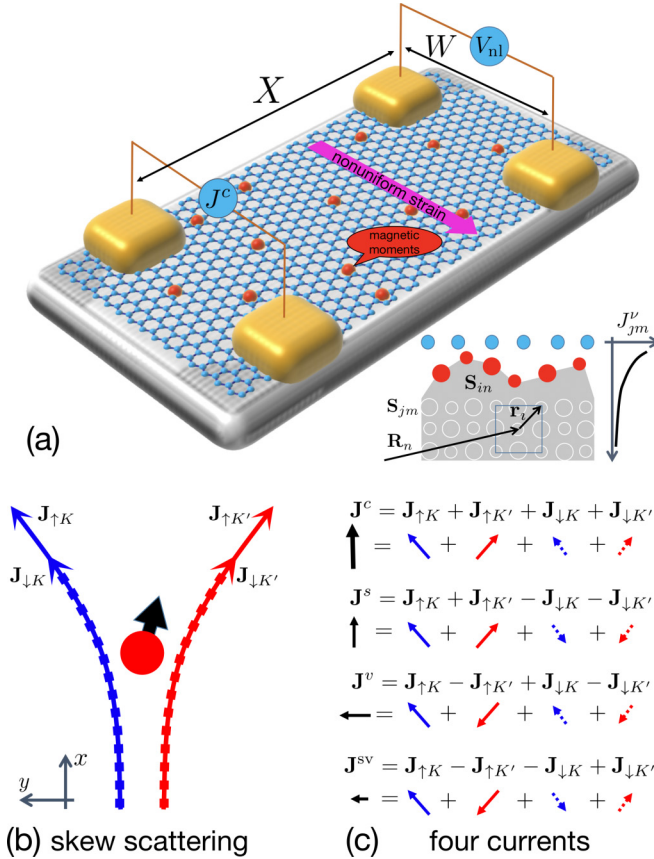


FIG. 1. (a) The sketch of a Hall bar device used for measuring nonlocal resistance in magnetized and strained graphene. Inset is the lateral view. The spin-exchange coupling J_{jm}^v in Eq. (4) decays fast away from the graphene layer, and hence the itinerant electrons merely interact with the interfacial magnetic moment (red circles). (b) The skew motion of the itinerant electrons in the magnetized and strained graphene. Here, the subscripts $s = \uparrow, \downarrow$ and $\tau = K, K'$ correspond to spin and valley degrees of freedom, respectively. (c) The summation of charge (J^c), spin (J^s), valley (J^v), and spin-valley (J^{sv}) currents. When we inject a charge current between two opposite left-hand-side contacts of the device, valley and spin-valley Hall currents emerge and diffuse along the channel due to the valley and spin-valley Hall effects, respectively. Both are converted back into the charge current via the inverse valley and spin-valley Hall effects, which leads to a charge accumulation and a nonlocal voltage on the right-hand side of the device. The nonlocal resistance R_{nl} is defined as the ratio of the voltage detected on the right side V_{nl} and the injection current on the left side J^c , i.e., $R_{nl} \equiv V_{nl}/J^c$.

Section V summarizes our findings. Finally, Appendix B gives the detailed derivations of the nonlocal resistance, and Appendix C shows the result of the antiferromagnetic case.

II. MODEL

The setup plotted in Fig. 1 is a Hall bar device made up of strained graphene on the top of a magnetic insulator [4–7]. The total Hamiltonian of the hybrid itinerant electron and magnetic moment system is

$$H = H_e + H_m + V_{em}. \quad (1)$$

Within the $\mathbf{k} \cdot \mathbf{p}$ approximation, the nonuniform strain produces a pseudogauge field that points to the opposite directions at opposite valleys K and K' [38–41]

$$H_e[\mathbf{k} - \tau^z \mathcal{A}(\mathbf{r})] = \hbar v_F [s^o \tau^z \sigma^x (k_x - e\tau^z \mathcal{A}_x) + s^o \sigma^y (k_y - e\tau^z \mathcal{A}_y)]. \quad (2)$$

\hbar is the reduced Planck constant, v_F is the Fermi velocity, e is charge of electron, and \mathbf{k} is kinetic momentum. s^w , σ^w , and τ^w are the Pauli matrices for the spin, sublattice, and valley degrees of freedom of itinerant electron with $w = o, x, y, z$, respectively, where $w = o$ corresponds to 2×2 identity matrix. The pseudogauge field reads $\mathcal{A}(\mathbf{r}) \simeq \frac{2}{ae}(u_{xx} - u_{yy}, -2u_{xy})$, where $u_{ij} = \frac{1}{2}(\partial_i u_j + \partial_j u_i)$ is strain tensor, \mathbf{u} is displacement field, and a is the carbon-carbon distance of graphene without strain [39]. We derive the thermodynamics of the magnetic insulator from the Heisenberg Hamiltonian

$$H_m = g_{in} \mu_B \hat{\mathbf{b}} \cdot \mathbf{S}_{in} - \frac{1}{2} J_{in,jm} \mathbf{S}_{in} \cdot \mathbf{S}_{jm}. \quad (3)$$

Hereafter, the repeated indices imply summation over. μ_B is the Bohr magneton, \mathbf{B} is a uniform external magnetic field in $\hat{\mathbf{b}} = \mathbf{B}/B$ direction, and g_{in} is the g factor for the unit cell n and sublattice i . $\mathbf{S}_{in} = (S_{in}^x, S_{in}^y, S_{in}^z)$ is the spin- S_i^o operator situated on unit cell n of sublattice i and $J_{in,jm} = J(\mathbf{r}_{in} - \mathbf{r}_{jm})$ is the exchange energy between spins situated on $\mathbf{r}_{in} = \mathbf{R}_n + \mathbf{r}_i$ and $\mathbf{r}_{jm} = \mathbf{R}_m + \mathbf{r}_j$, where \mathbf{R}_n is the replacement of unit cell n and \mathbf{r}_i is the replacement of sublattice i [inset of Fig. 1(a)].

The challenge of this work arises from the spin exchange between the itinerant electrons of the graphene and the d- or f-shell electrons of the magnetic atoms [42–44]

$$V_{em} = -\frac{1}{2} K_{in}^\alpha S_{in}^\alpha s^\alpha \delta(\mathbf{r} - \mathbf{r}_{in}). \quad (4)$$

The Greek superscript α sums over four components, where K_{in}^o describes the scalar potential and K_{in}^a describes the strength of the Kondo-type interaction with $a = (x, y, z)$. K_{in}^α decays fast away from graphene layer [inset of Fig. 1(a)]. Therefore, only the interfacial magnetic moments [red circles in Fig. 1(a)] interact with the itinerant electrons in the graphene. The interfacial magnetic moments can be assumed to be randomly distributed due to the imperfect magnetic interface but maintain their spin-spin coupling [45].

III. THEORY

A. Spin-relaxation anisotropy in a magnetized graphene

We microscopically derive the spin-relaxation time of the magnetized graphene within the random impurity, Born-Markov, and Weiss-field approximations [45,46]. The spin-relaxation time of longitudinal ($s^\parallel = s \cdot \hat{\mathbf{b}}$) and transverse [$s^\perp = \hat{\mathbf{b}} \times (s \times \hat{\mathbf{b}})$] spin components can be expressed in terms of the spin-spin correlators of the magnetic insulator and the microscopic parameters of the magnetic interface (see the detailed derivations in Appendix A 2)

$$\frac{1}{\tau_\parallel} = \frac{1}{\tau_0} + \frac{\pi}{4\hbar} \sum_j n_j v_F (K_j^s)^2 \beta \epsilon_L^j n_B(\epsilon_L^j) [1 + n_B(\epsilon_L^j)] |\langle S_j^\parallel \rangle|, \quad (5)$$

$$\frac{1}{\tau_\perp} = \frac{1}{2\tau_0} + \frac{1}{2\tau_\parallel} + \frac{\pi}{8\hbar} \sum_j n_j v_F (K_j^s)^2 \langle S_j^\parallel S_j^\parallel \rangle. \quad (6)$$

$S_j^\parallel = S_j \cdot \hat{\mathbf{b}}$ is the spin operator in the magnetic-field direction of sublattice j and n_j is the density of the interfacial magnetic moments of sublattice j . $n_B(\epsilon_L^j) = 1/(e^{\beta\epsilon_L^j} - 1)$ is the Bose-Einstein distribution function at temperature $\beta = 1/(k_B T)$ and effective Larmor frequency $\epsilon_L^j = g_j \mu_B B - \sum_{in} J_{in,jm} \langle S_{in}^\parallel \rangle$. τ_0 is the spin-relaxation time arising from intrinsic and extrinsic spin-orbit coupling as well as static disorders, which is assumed to be isotropic and independent of magnetic field and temperature. Here, we exclude the feedback effect of the itinerant electrons on the thermodynamic equilibrium state of the magnetic moments. Besides, we assume that the interfacial magnetic moments have the same thermodynamic equilibrium state as the bulk ones. Furthermore, it is assumed that all of the atoms on sublattice i are identical with $g_{in} = g_i$, $K_{in}^o = K_i^o$, $K_{in}^a = K_i^a$, $\langle S_i^a \rangle = \langle S_{in}^a \rangle$, and $\langle S_{in}^a S_{in}^a \rangle = \langle S_{in}^a S_{in}^a \rangle$ with $a = (x, y, z)$.

Let us study the spin anisotropy of both strongly and weakly magnetized regimes of magnetic insulators. The former happens at a low enough temperature or strong enough field in a paramagnetic insulator, at low enough temperature ($T \ll T_C$) in a ferromagnetic insulator, as well as at low enough temperature ($T \ll T_N$) in an antiferromagnetic insulator, where T_C (T_N) is the critical (Neel) temperature of ferromagnetic (antiferromagnetic) insulator. In the strongly magnetized regime, spins of the magnetic moments are frozen and spin flip is prohibited. Thus, the spin-relaxation time (5) and (6) reduces $\tau_{\parallel}^{-1} = \tau_0^{-1}$ and $\tau_{\perp}^{-1} = \tau_0^{-1} + \sum_j \Omega_0^j$, respectively, where $\Omega_0^j = \frac{\pi}{\hbar} n_j v_F (K_j^s S_j^o)^2$. Then, we reach the most anisotropic case with $\langle S_j^\parallel \rangle = -S_j$ and $\langle S_j^\perp \rangle = \mathbf{0}$. In the opposite limit, where the microscopic magnetic order is fully destroyed, the spin-relaxation time (5) and (6) reduces $\tau_{\parallel}^{-1} = \tau_{\perp}^{-1} = \tau_0^{-1} + \sum_j \Omega_1^j$, where $\Omega_1^j = \frac{2\pi}{3\hbar} v_F (n_j K_j^s K_j^s) S_j^o (S_j^o + 1)$. Thus, we reach isotropic case with $\langle S_j^\parallel \rangle = 0$ and $\langle S_j^\perp \rangle = \mathbf{0}$.

B. Extrinsic spin-valley Hall effect in a magnetized and strained graphene

We present the spin-diffusion formalism in strained and magnetized graphene. In the diffusive regime [47–51], we describe the transport of spin and valley degrees of freedom of itinerant electrons with the system of drift-diffusion equations [22] derived microscopically from the Boltzmann equation [37,52,53] or the Kubo formalism [54,55]

$$D \partial_i N^\mu - \sigma \delta^{\mu c} E_i^\mu = [-\delta^{\mu\nu} \delta_{ij} + (R)_{ij}^{\mu\nu}] J_j^\nu. \quad (7)$$

The Latin subscripts refer to the spatial component, i.e., $\{i, j\} \in \{x, y\}$, while the Greek superscripts ν and μ sum over the set $\{c, s, v, sv\}$, which correspond to the charge (c), spin (s), valley (v), and spin-valley (sv) current J_j^ν (density N^μ) of the itinerant electrons, respectively. $\delta^{\mu\nu}$ and δ_{ij} are Dirac delta functions. The spin density and current are polarized in the direction of the external magnetic field ($s^\parallel = s \cdot \hat{\mathbf{b}}$), and hence there is no spin precession (i.e., Hanle effect). The left-hand side of Eq. (7) includes the diffusion current from spatial nonuniformity of the densities $-D \partial_i N^\mu$ and the drift current from the generalized electric fields σE_i^μ , where $E_i^\mu = 0$ for all $\mu \neq c$ in typical spintronic materials. $\sigma = ne^2 \tau / m$ is the Drude conductivity and $D = v_F^2 \tau / 2$ is the diffusion constant,

where m , n , and τ are the electron mass, the electron density, and the momentum relaxation time of the magnetized and strained graphene, respectively. Hereafter, we consider the case of $K_j^o \gg K_j^s$ for simplicity and hence the momentum relaxation time is dominated by the scalar potential $\tau^{-1} \simeq \frac{\pi}{8\hbar} \sum_j n_j v_F (K_j^o S_j^o)^2$.

The right-hand side of Eq. (7) is current relaxation. We describe the coupling of different currents with a resistivity matrix

$$(R)_{ij}^{\mu\nu} = \omega_s \tau \delta_{ij} \begin{bmatrix} 0 & 1 & 0 & 0 \\ 1 & 0 & 0 & 0 \\ 0 & 0 & 0 & 1 \\ 0 & 0 & 1 & 0 \end{bmatrix} + \omega_v \tau \epsilon_{ij} \begin{bmatrix} 0 & 0 & 1 & 0 \\ 0 & 0 & 0 & 1 \\ 1 & 0 & 0 & 0 \\ 0 & 1 & 0 & 0 \end{bmatrix} \begin{matrix} c \\ s \\ v \\ sv \end{matrix}. \quad (8)$$

We have introduced the Dirac delta (δ_{ij}) and the 2D Levi-Civita (ϵ_{ij}) tensors in symmetric and antisymmetric resistivity matrices, respectively. The symmetric resistivity matrix couples the charge (c , first row) and valley currents (v , third row) to spin (s , second row) and spin-valley (sv , fourth row) currents, respectively. This kind of coupling can originate from the interplay of the scalar potential and the Kondo-type interaction [Eq. (4)], parameterized by the spin-scattering rate (see the detailed derivations in Appendix A 1)

$$\omega_s \simeq \frac{\pi}{4\hbar} \sum_j n_j v_F K_j^o K_j^s S_j^o |\langle S_j^\parallel \rangle|. \quad (9)$$

v_F is the density of the state of the graphene. On the other hand, the asymmetric resistivity matrix couples the charge (c , first row) and spin (s , fourth row) to the valley (v , third row) and spin-valley currents (sv , second row) currents, respectively. This kind of coupling arises from nonuniform strain and results in strong pseudovalley magnetic field $\mathcal{B}_v = \nabla \times \mathcal{A}_v$ [56]. It induces an effective valley Lorentz force [37,57,58], similar to spin Lorentz force from the spin-orbit coupling [59,60]. We parametrize the valley magnetic field \mathcal{B}_v by valley cyclotron frequency [22,37]

$$\omega_v = \frac{e v_F}{2m} \mathcal{B}_v. \quad (10)$$

The pseudovalley magnetic field has been assumed to be spatially uniform for simplicity.

The spin and valley transport of the magnetized and strained graphene can be intuitively understood by the skew scattering plotted in Fig. 1(b). In the presence of the strain-induced valley magnetic field [Eq. (10)], the valley- K electrons are deflected to the right, while the valley- K' electrons are deflected to the left. A valley current emerges in the transverse direction. In the presence of the spin-dependent scattering [Eq. (9)], we reach a spin-resolved skew scattering, which results in longitudinal spin current and transverse spin-valley current [Figs. 1(b) and 1(c)]. We solve Eq. (7) in the spatial uniform case, where $\partial_j N^\mu = 0$. The ratio of the longitudinal spin current J^s , transverse valley current J^v , and transverse spin-valley current J^{sv} over the longitudinal charge

current J^c are dubbed as charge-to-spin efficiency, valley Hall angle, and spin-valley Hall angle, respectively,

$$\eta_s(B, T) = \frac{1 - (\omega_v \tau)^2 + (\omega_s \tau)^2}{1 + (\omega_v \tau)^2 + (\omega_s \tau)^2} (\omega_s \tau), \quad (11)$$

$$\theta_v(B, T) = \frac{1 + (\omega_v \tau)^2 - (\omega_s \tau)^2}{1 + (\omega_v \tau)^2 + (\omega_s \tau)^2} (\omega_v \tau), \quad (12)$$

$$\theta_{sv}(B, T) = \frac{2(\omega_s \tau)(\omega_v \tau)}{1 + (\omega_s \tau)^2 + (\omega_v \tau)^2}. \quad (13)$$

The interplay of strain and magnet not only results in the renormalization of the charge-to-spin conversion [Eq. (11)] and the valley Hall effect [Eq. (12)] but also leads to the emergence of the SVHE [Eq. (13)]. Note that θ_{sv} is proportional to both $\omega_v \tau$ and $\omega_s \tau$, and hence it is nonzero only if both magnet and strain coexist. The formation of the spin-valley Hall current is a two-stage process requiring the generation of a longitudinal spin (transverse valley) current from driving electric current via the magnet (strain). The resulting currents are then converted into a transverse spin-valley current by strain (magnet).

Then, we present a convenient way to detect the extrinsic SVHE. Being electrically neutral, direct detection of spin-valley Hall current is not possible. Its existence must be inferred by indirect means such as nonlocal transport measurements performed on a Hall bar device as depicted in Fig. 1(a). When we drive an electric current between the two opposite left-hand-side contacts of the Hall bar device, both valley and spin-valley Hall currents emerge and diffuse in the transverse direction to the applied electric current. Then, they are converted back into electric current by the inverse valley and spin-valley Hall effects, which leads to a charge accumulation and a nonlocal voltage on the right-hand side of the device. The nonlocal resistance R_{nl} is defined as the ratio of the nonlocal voltage V_{nl} to the external current applied to the device J^c , such that $R_{nl} = V_{nl}/J^c$. In typical spintronic materials, the charge-to-spin efficiency is small $\omega_s \tau \ll 1$ [62], while the nonuniform strain in graphene can yield large valley Hall angle $\omega_v \tau \gg \omega_s \tau$ ($\omega_v \tau \sim 1$ [37]). Therefore, the nonlocal resistance from the valley Hall effect is much larger than the contribution from the SVHE. To have sizable SVHE, we are required to tune the strain level such that $\omega_v \tau \simeq 1$ and the spin-valley Hall angle reach its maximum $\theta_{sv} \simeq \omega_s \tau$ [see Eq. (13)]. In this case, the charge-to-spin efficiency $\eta_s = (\omega_s \tau)^3/2$ is negligibly small [see Eq. (11)] and transverse modes, valley and spin-valley densities, are decoupled and can independently propagate along the Hall bar [see Eq. (B2) in Appendix B]. We are interested in the magnetic field and temperature dependence of the nonlocal resistance induced by the SVHE (see detailed derivation in Appendix B)

$$R_{nl}^{sv}(B, T) \simeq \theta_{sv}^2 \frac{W}{2\ell_{sv}} \rho e^{-|X|/\ell_{sv}}. \quad (14)$$

X and W are the length and width of the Hall bar device, respectively [Fig. 1(a)]. $\ell_{sv} = \sqrt{D\tau_{sv}}$ is spin-valley diffusion length. Both spin- and valley-flip scattering result in spin-valley-flip scattering. Hence, spin-valley relaxation time reads $\tau_{sv}^{-1} = \tau_{\parallel}^{-1} + \tau_{vf}^{-1}$, where τ_{vf} includes the

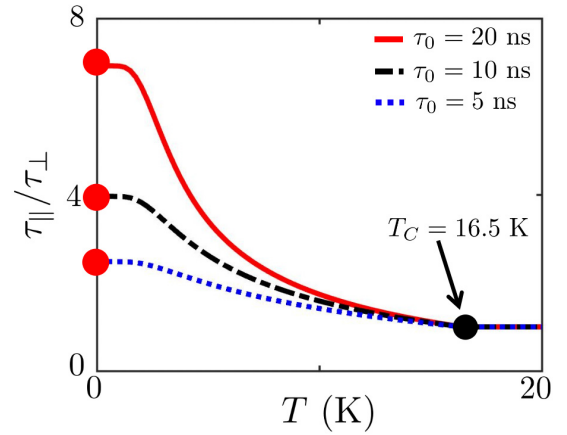


FIG. 2. Anisotropic spin relaxation described by the ratio $\tau_{\parallel}/\tau_{\perp}$ [Eqs. (5) and (6)] as a function of temperature, T for different intrinsic spin-relaxation times τ_0 , where $B \rightarrow 0$ T. Here, ferromagnetic substrate is chosen as EuS with the Curie temperatures $T_C = 16.5$ K [61]. At low enough temperature ($T \ll T_C$), all spins within the ferromagnetic insulator are frozen and spin flip is prohibited. Hence, the ratio of longitudinal and transverse spin relaxation reads $\tau_{\parallel}/\tau_{\perp} = 1 + \Omega_0 \tau_0$ (red circles). At the temperature $T > T_C$, the magnetic order is fully destroyed and the spin-flip procedure dominates. Thus, the spin-relaxation time (5) and (6) reduces $\tau_{\parallel}^{-1} = \tau_{\perp}^{-1} = \tau_0^{-1} + \Omega_1$ and we reach isotropic case, i.e., $\tau_{\parallel}/\tau_{\perp} = 1$ (black circle).

contribution from the valley-flip scattering from the short-region of disorders [37].

IV. RESULTS AND DISCUSSIONS

The magnetic and thermal properties of the spin and valley transport in the magnetized graphene greatly rely on the microscopic magnetic ordering within the magnetic insulators. The numerous magnetic configurations of the magnetic moments such as paramagnet [63], ferromagnet [64], ferrimagnet, and antiferromagnet provide multiple behaviors of spin relaxation [Eqs. (5) and (6)] and nonlocal resistance [Eq. (14)]. Hereafter, we focus on the ferromagnetic insulator for simplicity. There exists only one sublattice. Thus, we can remove subscript j in Eqs. (5), (6), and (9). We study EuS with Curie temperature $T_C = 16.5$ K [61], large exchange coupling (~ 10 meV), and large magnetic moment per Eu ion ($\sim 7\mu_B$) [65]. We also study the antiferromagnetic case in Appendix C, which is a special case of ferrimagnet.

Let us begin with the temperature dependence of spin-relaxation anisotropy induced by the ferromagnetic insulator. Prior work on spin anisotropy mainly focused on the spin-orbit interaction [66,67]. Recently, a giant spin-relaxation anisotropy has been reported in graphene in proximity to transition-metal dichalcogenides [68–72]. Alternatively, we here achieve strongly anisotropic spin relaxation by ferromagnetic proximity effect. Here, we express the spin-relaxation time, as shown in Eqs. (5) and (6), in terms of the microscopic parameters of the magnetic interface as well as the magnetization and spin-spin correlators of the magnetic moments. Figure 2 plots the ratio of longitudinal and transverse spin-relaxation time $\tau_{\parallel}/\tau_{\perp}$ as a function of temperature T in the limit of $B \rightarrow 0$. At low enough temperature ($T \ll T_C$),

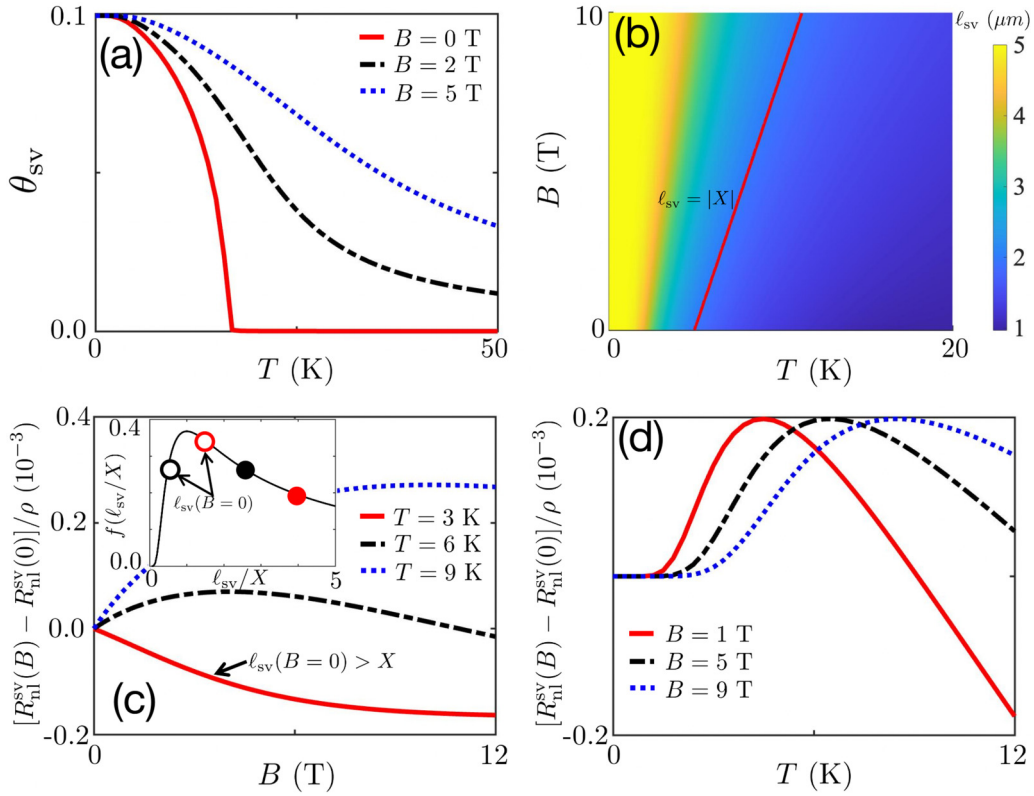


FIG. 3. The out-of-plane magnetic field and temperature dependence of SVHE for EuS substrate with Curie temperature $T_C = 16.5$ K [61]. (a) Spin-valley Hall angle, θ_{sv} as a function of temperature T (K) [Eq. (13)]. (b) Spin-valley diffusion length ℓ_{sv} as a function of temperature T and field B . The red line corresponds to $\ell_{sv} = X$ and the color bar is in the unit of μm . (c), (d) Relative nonlocal resistance of ferromagnetic substrate, $[R_{nl}^{sv}(B) - R_{nl}^{sv}(0)]/\rho$, as a function of (c) magnetic field B and (d) temperature T [Eq. (14)]. Inset of (c) plots $f(\ell_{sv}/X) = \frac{X}{\ell_{sv}} e^{-X/\ell_{sv}}$ as a function of ℓ_{sv}/X . The red line in (b) corresponds to $\ell_{sv} = |X|$. We find that positive and negative nonlocal magnetoresistance correspond to $\ell_{sv} < |X|$ and $\ell_{sv} > |X|$, respectively [(c)]. This also results in a maximum of nonlocal resistance as a function of T [Fig. 3(d)]. Other parameters: $\ell_{sv}^{\max} = 5\mu\text{m}$, $\ell_{sv}^{\min} = 1\mu\text{m}$, $X = 2\mu\text{m}$, $W = 1\mu\text{s}$, and $K^s/K^o = 0.05$.

i.e., the fully magnetized regime, all spins within the ferromagnetic insulator are frozen, and spin flip is prohibited. Hence, the ratio of longitudinal and transverse spin relaxation reads $\tau_{\parallel}/\tau_{\perp} = 1 + \Omega_0\tau_0$. As shown in Fig. 2, the larger τ_0 corresponds to the stronger anisotropy (at $T \rightarrow 0$ K). With increasing temperature, the spin flip of itinerant electrons caused by the ferromagnetic insulator is allowed. At the temperature $T > T_C$, the magnetic order is fully destroyed and the spin-flip procedure dominates. Thus, the spin-relaxation time (5) and (6) reduces to $\tau_{\parallel}^{-1} = \tau_{\perp}^{-1} = \tau_0^{-1} + \Omega_1$ and we reach the isotropic case.

We study the out-of-plane magnetic field¹ and the temperature dependence of the nonlocal resistance [Eq. (14)] to prove the existence of the SVHE. This dependence can extract the nonlocal resistance from the valley Hall effect, which is independent of magnetic field and temperature. Second, the ordinary Hall effect is negligible because the ordinary Hall angle $\propto \tau B$ ($B \sim 10$ T) is much smaller than the valley Hall angle $\propto \tau B_v$ ($B_v \sim 300$ T [56]) for small enough τ in the diffusive limit. Third, we exclude the Hanle effect, that is,

¹In principle, we also use the in-plane magnetic field. The spin Hall effect with an out-of-plane spin polarization will decay fast due to the short spin diffusion length induced by the magnetic moments.

the oscillation of the nonlocal resistance as a function of an in-plane magnetic field [47,48,53,73]. From Eq. (14), there are two origins of the magnetic field and the temperature dependence of nonlocal resistance, spin-valley Hall angle [Eq. (13) and Fig. 3(a)] and diffusion length [Eq. (5) and Fig. 3(b)]. For the case of the ferromagnetic insulator EuS, with one sublattice, the spin-valley Hall angle, $\theta_{sv} = (2K^s \langle S_{\parallel} \rangle) / (K^o S^o)$, is proportional to the spin expectation $\langle S_{\parallel} \rangle$. The temperature dependence of spin-valley Hall angle θ_{sv} is plotted in Fig. 3(a) for different magnetic field. In the limit of $B \rightarrow 0$ T, we observe that $\theta_{sv} = 0$ for $T > T_C$. Figure 3(b) plots the spin-valley diffusion length ℓ_{sv} as a function of field B and temperature T , which monotonically increases (decreases) with B (T). In the low-temperature limit, it reaches its maximum $\ell_{sv}^{\max} = \sqrt{D\tau_0}$, which depends on both isotropic spin- and valley-flip scattering irrelevant to EuS. In high-temperature limit, spin-valley diffusion length reaches its minimum $\ell_{sv}^{\min} = \sqrt{D\tau_0 / (1 + \Omega_1\tau_0)}$, which relies on the density of magnetic moments and spin exchange coupling. The magnetic field modulation of the spin-valley Hall angle [Fig. 3(a)] and diffusion length [Fig. 3(b)] reveals a new mechanism of the nonlocal magnetoresistance effect.

Next, we discuss the magnetic and thermal properties of nonlocal resistance. To exclude the large nonlocal resistance from the valley Hall effect, Figs. 3(c) and 3(d) plot the

relative nonlocal resistance of the ferromagnetic substrate, $[R_{\text{nl}}(B) - R_{\text{nl}}(0)]/\rho$, as a function of (c) magnetic field B and (d) temperature T [Eq. (14)]. For $\ell_{\text{sv}}^{\text{min}} < |X| < \ell_{\text{sv}}^{\text{max}}$, we expect a maximum of nonlocal resistance, as shown in Figs. 3(c) and 3(d). It happens around $\ell_{\text{sv}} = |X|$ [red line in Fig. 3(b)]. To better understand this behavior, let us assume spin-valley Hall angle θ_{sv} is independent of the magnetic field and temperature for simplicity. Then, the relative nonlocal resistance is proportional to a function $f(\ell_{\text{sv}}/X) = \frac{X}{\ell_{\text{sv}}} e^{-X/\ell_{\text{sv}}}$, which monotonically increases for $\ell_{\text{sv}}/X \in (0, 1)$ and monotonically decreases for $\ell_{\text{sv}}/X \in (1, \infty)$ [inset of Fig. 3(c)]. Increasing magnetic field or reducing temperature inhibits spin-valley flip (or spin flip) and results in longer spin-valley diffusion length [Fig. 3(b)]. For the zero-field spin-valley length $\ell_{\text{sv}}(B=0)$ smaller than X [black circles of the inset of Fig. 3(c)], increasing magnetic field first enhances the relative nonlocal resistance for $\ell_{\text{sv}} < X$, and then lessens the relative nonlocal resistance for $\ell_{\text{sv}} > X$. The position of this maximum is dependent on X , B , and T , as shown in Figs. 3(b) and 3(d). If we begin with a low enough temperature ($T \ll T_C$) that $\ell_{\text{sv}}(B=0) > X$ [red circles of the inset of Fig. 3(c)], the relative nonlocal resistance monotonically decreases with the magnetic field [red line in Fig. 3(c)]. This roughly estimates the spin-valley diffusion length, where positive and negative nonlocal magnetoresistance correspond to $\ell_{\text{sv}} < |X|$ and $\ell_{\text{sv}} > |X|$, respectively. This criterion is obtained when we omit the influence of the magnetic field and temperature dependence from θ_{sv} , which only leads to a small shift of the location of maximum. Using the experimentally feasible parameters, we obtain the relative nonlocal resistance $[R_{\text{nl}}^{\text{sv}}(B) - R_{\text{nl}}^{\text{sv}}(0)]/\rho \sim 10^{-3}$, that is, $[R_{\text{nl}}^{\text{sv}}(B) - R_{\text{nl}}^{\text{sv}}(0)] \sim 1\Omega$ for $\rho \sim 1000\Omega$ [16,48], which is observable for current techniques [16,47–49].

V. CONCLUSION AND OUTLOOK

In conclusion, we demonstrate the extrinsic spin-valley Hall effect by the magnetic field and temperature modulation of nonlocal resistance in magnetized and strained graphene. The rich magnetic field and temperature dependencies from different magnetic ordering within materials allow for fruitful control of the spin-valley Hall effect and demonstrate its existence by nonlocal resistance in the Hall bar device. We achieve a striking crossover from positive to negative nonlocal magnetoresistance owing to the magnetic field dependence of spin-valley relaxation rather than spin precession. In addition, we determine the giant spin-relaxation anisotropy due to the ferromagnetic insulator, which also works on the magnetic semiconductors [74–76]. Though we concentrate on the spin-valley Hall effect, the magnetic field dependence of the spin-relaxation time also offers a new modulation of nonlocal resistance instead of the usual Hanle spin precession [47,48,77]. The physical understanding of spin relaxation in semiconductors plays a crucial role in the current development of spin-based electronics [78] and spin-based quantum computation [79].

ACKNOWLEDGMENTS

We thank Pierre Fromholz, Zhe Hou, Zhe Yuan, Shun-Qing Shen, and Miguel Angel Cazalilla for helpful discussions.

This project has received funding from the Spanish Ministerio de Ciencia e Innovacion (MICINN) through Project No. FIS2017-82804-P.

APPENDIX A: MAGNETIC IMPURITY

In this section, we derive the spin-scattering rate [Eq. (9) of the main text] and spin-relaxation time [Eqs. (5) and (6) of the main text]. We study the spin-dependent scattering and spin-relaxation time of the itinerant electrons of the graphene in the presence of the interfacial magnetic moments of the magnetic insulator. The calculation of the spin-relaxation time from magnetic moments itself is already a challenge. During the derivation of scattering and relaxation time, we have made the following two assumptions for simplicity. First, we excluded the feedback effect of the itinerant electrons on the thermodynamic equilibrium state of the magnetic moments and assume that the interfacial magnetic moments have the same thermodynamic equilibrium state as the bulk ones described by the Heisenberg Hamiltonian (3) in the main text. The resulted magnetized graphene Hamiltonian is given by

$$H = H_e + V_{\text{em}}. \quad (\text{A1})$$

Here, we did not add the Hamiltonian of the local moments, because it will not influence the calculation of spin scattering and relaxation time. Second, we omit the effect of the strain on the spin scattering and relaxation time. Thus, during the derivation of spin-relaxation time, we use the Hamiltonian of the pristine graphene

$$H_e = \hbar v_F (k_x s^o \tau^z \sigma^x + k_y s^o \tau^o \sigma^y). \quad (\text{A2})$$

\hbar is the reduced Planck constant, v_F is the Fermi velocity, e is charge of electron, and \mathbf{k} is kinetic momentum. s^w , σ^w , and τ^w are the Pauli matrices for the spin, sublattice, and valley degrees of freedom of itinerant electron with $w = o, x, y, z$, respectively, where $w = o$ corresponds to 2×2 identity matrix. Obviously, spin (s) and valley (τ) are good quantum numbers and we can easily obtain eigenstates and eigenvalues of the pristine Hamiltonian

$$E_{\eta\mathbf{k}}^{s\tau} = \eta \sqrt{k_x^2 + k_y^2}, \quad (\text{A3})$$

$$|E_{\eta\mathbf{k}}^{s\tau}\rangle = \zeta_s \zeta_\tau \frac{1}{\sqrt{2}} \begin{bmatrix} \tau e^{-i\tau\theta_{\mathbf{k}}/2} \\ \eta e^{+i\tau\theta_{\mathbf{k}}/2} \end{bmatrix}. \quad (\text{A4})$$

In the position representation, the wave function of the eigenstate (A4) reads

$$\langle \mathbf{r} | E_{\eta\mathbf{k}}^{s\tau} \rangle = \frac{1}{\sqrt{\Omega}} e^{+ik\cdot\mathbf{r}} \zeta_s \zeta_\tau \frac{1}{\sqrt{2}} \begin{bmatrix} \tau e^{-i\tau\theta_{\mathbf{k}}/2} \\ \eta e^{+i\tau\theta_{\mathbf{k}}/2} \end{bmatrix}. \quad (\text{A5})$$

Hereafter, we set the area of graphene Ω equal to 1. Obviously, $|E_{\eta\mathbf{k}}^{s\tau}\rangle$ is not depended on the magnitude of kinetic momentum $|k|$. The spin-dependent scattering arises from the spin exchange between the itinerant electrons of the graphene and the d- or f-shell electrons of the magnetic atoms [42–44]

$$V_{\text{em}}(\mathbf{r}) = -\frac{1}{2} \sum_{i\alpha} K_i^\alpha S_{in}^\alpha s^\alpha \delta(\mathbf{r} - \mathbf{r}_{in}). \quad (\text{A6})$$

$S_{in} = (S_{in}^x, S_{in}^y, S_{in}^z)$ is the spin- S_i^o operator situated on unit cell n of sublattice i . K_i^o describes the scalar potential and

K_i^a describes the strength of the Kondo-type interaction with $a = (x, y, z)$. Hereafter, we consider the case of $K_i^o \gg K_i^s$ for simplicity.

1. Charge-to-spin conversion

In this section, we study the charge-to-spin conversion up to the first order of K_i^s . In this case, the spins of the magnetic momentum can be treated as classical spin and Eq. (A6) reduces into

$$V_{\text{em}}(\mathbf{r}) = -\frac{1}{2} \sum_{\alpha=o,s} \sum_{in} K_i^\alpha \langle S_{in}^\alpha \rangle s^\alpha \delta(\mathbf{r} - \mathbf{r}_{in}). \quad (\text{A7})$$

$s = \uparrow, \downarrow$ correspond to spin up and down polarized in the direction of the external magnetic field, respectively. Then, we consider the spin- and energy-conserved scattering. The transition rate from $|E_{\eta p}^{s\tau}\rangle$ to $|E_{\eta k}^{s\tau}\rangle$ is given by

$$w_{\mathbf{k} \leftarrow \mathbf{p}}^s = -\frac{1}{2} \sum_{jm} (K_j^o S_j^o + s K_j^s \langle S_j^z \rangle) \cos\left(\frac{\theta_p - \theta_k}{2}\right) \times e^{i(\mathbf{k}-\mathbf{p}) \cdot \mathbf{r}_{jm}}, \quad (\text{A8})$$

and we obtain the spin-dependent scattering probability

$$W_s(\mathbf{k} - \mathbf{p}) = \frac{1}{4} \sum_{ijnm} (K_j^o S_j^o + s K_j^s \langle S_j^z \rangle) (K_i^o S_i^o + s K_i^s \langle S_i^z \rangle) \times \cos^2\left(\frac{\theta_p - \theta_k}{2}\right) e^{i(\mathbf{k}-\mathbf{p}) \cdot (\mathbf{r}_{in} - \mathbf{r}_{jm})}. \quad (\text{A9})$$

After the conventional impurity averaging, the spin-dependent scattering probability (A9), up to the first order of n_j and K_j^s , reduces to

$$W_s(\mathbf{k} - \mathbf{p}) \simeq \frac{1}{4} \sum_j n_j [(K_j^o S_j^o)^2 + 2s K_j^o K_j^s \langle S_j^z \rangle] \times \cos^2\left(\frac{\theta_p - \theta_k}{2}\right). \quad (\text{A10})$$

The collision integral of each spin species reads

$$I[f_{\eta k}^{s\tau}] = -\frac{2\pi}{\hbar} \sum_p W_s(\mathbf{k} - \mathbf{p}) \delta(E_{\eta k} - E_{\eta p}) (f_{\eta k}^{s\tau} - f_{\eta p}^{s\tau}). \quad (\text{A11})$$

$f_{\eta k}^{s\tau}$ is the distribution function of graphene electrons. In equilibrium, we reach

$$f_{\eta k}^{s\tau, \text{eq}} = f(E_{\eta k}) = \frac{1}{e^{\beta(E_{\eta k} - \mu_F)} + 1}. \quad (\text{A12})$$

$f(E)$ is the Fermi-Dirac distribution function with chemical potential μ_F and temperature $\beta = 1/k_B T$, where k_B is the Boltzman constant and T is the temperature. Obviously, we have $I_s[f_{\eta k}^{s\tau, \text{eq}}] = 0$. For small electric field, \mathbf{E} , the distribution is not much different from the equilibrium ones $f_{\eta k}^{s\tau} = f_{\eta k}^{s\tau, \text{eq}} + \delta f_{\eta k}^{s\tau}$, with $f_{\eta k}^{s\tau, \text{eq}} \gg \delta f_{\eta k}^{s\tau}$. In the lowest order of \mathbf{E} , we have the following ansatz:

$$\delta f_{\eta k}^{s\tau} = (\mathbf{k} \cdot \mathbf{E}) F_s(E_{\eta k}). \quad (\text{A13})$$

By substitution of Eq. (A13), the collision term (A11) becomes

$$I[\delta f_{\eta k}^{s\tau}] = -\frac{2\pi}{\hbar} \int_{-\pi}^{+\pi} \frac{d\theta_p}{2\pi} v(E_{\eta k}) W_s\left(\frac{\theta_p - \theta_k}{2}\right) \times [\cos(\theta_k) - \cos(\theta_p)] k E F_s(E_{\eta k}). \quad (\text{A14})$$

where $v(E_{\eta k})$ is the density of state of the graphene at energy $E_{\eta k}$. Using the identity

$$\cos(\theta_p) = \cos(\theta_p - \theta_k) \cos(\theta_k) - \sin(\theta_p - \theta_k) \sin(\theta_k), \quad (\text{A15})$$

Eq. (A14) reduces to

$$I[\delta f_{\eta k}^{s\tau}] = -\frac{1}{\tau^s} \delta f_{\eta k}^{s\tau}. \quad (\text{A16})$$

The spin-dependent scattering rate is given by

$$\frac{1}{\tau^s} = \frac{2\pi}{\hbar} v_F \int_{-\pi}^{+\pi} \frac{d\theta}{2\pi} W_s\left(\frac{\theta}{2}\right) [1 - \cos(\theta)], \quad (\text{A17})$$

where v_F is the density of state of graphene at Fermi energy. The spin-dependent scattering rate (A17) can be divided into two parts

$$\frac{1}{\tau^s} = \frac{1}{\tau} - s\omega_s, \quad (\text{A18})$$

where the momentum relaxation time and spin scattering rate, respectively, are given by

$$\frac{1}{\tau} = \frac{\pi}{8\hbar} \sum_j n_j v_F (K_j^o S_j^o)^2, \quad (\text{A19})$$

$$\omega_s \simeq \frac{\pi}{4\hbar} \sum_j n_j v_F K_j^o K_j^s S_j^o |\langle S_j^z \rangle|, \quad (\text{A20})$$

where $\langle S_j^z \rangle \leq 0$. Then, the collision term (A11) becomes

$$I[\delta f_{\eta k}] = -\frac{1}{\tau} \delta f_{\eta k} + \omega_s \delta^z \delta f_{\eta k}, \quad (\text{A21})$$

with

$$\delta f_{\eta k} = \begin{bmatrix} \delta f_{\eta k}^{\uparrow\tau} & 0 \\ 0 & \delta f_{\eta k}^{\downarrow\tau} \end{bmatrix}. \quad (\text{A22})$$

The second term of the right-hand side of Eq. (A21) is responsible for the charge-to-spin conversion.

2. Spin-relaxation time

In this section, we study the spin-relaxation time up to second order K_j^s . We define spin states at the Bloch sphere with arbitrary coordinates (θ, ϕ) , where $\theta \in [0, \pi]$ and $\phi \in [0, 2\pi)$,

$$|\uparrow\rangle = \cos\left(\frac{\theta}{2}\right) |\uparrow\rangle - e^{-i\phi} \sin\left(\frac{\theta}{2}\right) |\downarrow\rangle, \quad (\text{A23})$$

$$|\downarrow\rangle = \cos\left(\frac{\theta}{2}\right) |\downarrow\rangle + e^{+i\phi} \sin\left(\frac{\theta}{2}\right) |\uparrow\rangle. \quad (\text{A24})$$

The Kondo-type spin exchange coupling in Eq. (A6) in the rotated spin basis (A23) and (A24) reads

$$V_{sd} = -\sum_i \frac{K_i^s}{2} \left\{ \frac{1}{2} [S_{+z}^i S_{-z}^i(\mathbf{r}) + S_{-z}^i S_{+z}^i(\mathbf{r})] + S_{2z}^i S_z(\mathbf{r}) \right\}, \quad (\text{A25})$$

with

$$S_+^{i,z} = S_x^i + iS_y^i, s_+^z(\mathbf{r}) = s_x(\mathbf{r}) + is_y(\mathbf{r}), \quad (\text{A26})$$

$$S_-^{i,z} = S_x^i - iS_y^i, s_-^z(\mathbf{r}) = s_x(\mathbf{r}) - i\sigma_y(\mathbf{r}). \quad (\text{A27})$$

where $i = (t, n)$. The first (second) term of the right-hand side of equation (A25) describes spin flip (split) in the rotated basis $|\uparrow\rangle$ and $|\downarrow\rangle$ with quantization Pauli matrix s_z .

The spin relaxation arises from the spin flip. The expression of the spin-relaxation time is given by [45]

$$\frac{1}{\tau_z} = \frac{2\beta}{v_F} \sum_{kp} W_{\downarrow\uparrow}^{\tau\eta}(\mathbf{p}, \mathbf{k}) f(E_{\eta\mathbf{k}}^{\uparrow\tau}) [1 - f(E_{\eta\mathbf{p}}^{\downarrow\tau})]. \quad (\text{A28})$$

Within impurity averaging, the Born-Markov, and the Weiss-field approximations, the rate for free electron transition from $|E_{\eta\mathbf{k}}^{\uparrow\tau}\rangle$ into momentum $|E_{\eta\mathbf{p}}^{\downarrow\tau}\rangle$ is given by

$$W_{\downarrow\uparrow}^{\tau\eta}(\mathbf{p}, \mathbf{k}) = \frac{\pi}{8\hbar^2} \sum_j n_j (K_j^s)^2 D_{-+}^{j,z}(E_{\eta\mathbf{k}}^{\uparrow\tau}/\hbar - E_{\eta\mathbf{p}}^{\downarrow\tau}/\hbar) \times \cos^2\left(\frac{\theta_{\mathbf{p}} - \theta_{\mathbf{k}}}{2}\right), \quad (\text{A29})$$

where $D_{-+}^{j,z}(\omega)$ is the Fourier transformation of the spin-spin correlation function $\langle S_{-+}^{j,z}(t) S_{-+}^{j,z} \rangle$.

The longitudinal spin-relaxation time corresponds to $\theta = 0$, $\phi = 0$. We have spin-flip operators $S_{-+}^{j,\parallel} = S_j^x + iS_j^y$ and $S_{-+}^{j,\perp} = S_j^x - iS_j^y$. Then, the spin-spin correlation function becomes

$$D_{-+}^{j,\parallel}(\omega) = 2[1 + n_B(\epsilon_L^j)] |\langle S_j^{\parallel} \rangle| \delta(\omega - \epsilon_L^j/\hbar), \quad (\text{A30})$$

where $n_B(E) = 1/(e^{\beta E} - 1)$ is the Bose-Einstein distribution function. $\epsilon_L^j = g_j \mu_B B - \sum_{jm} J_{jm,ln} \langle S_{ln}^z \rangle$ is the energy of Weiss field, where μ_B is the Bohr magneton, \mathbf{B} is a uniform external magnetic field, and g_{ln} is the g factor for the unit cell n and sublattice j . $J_{ln,jm}$ is the exchange energy between spins \mathbf{S}_{ln} and \mathbf{S}_{jm} . Thus, the longitudinal spin-relaxation time is given by

$$\frac{1}{\tau_{\parallel}} = \frac{\pi}{4\hbar} \sum_j n_j v_F (K_j^s)^2 \beta \epsilon_L^j n_B(\epsilon_L^j) [1 + n_B(\epsilon_L^j)] |\langle S_j^{\parallel} \rangle|, \quad (\text{A31})$$

where we use the integral formula

$$\int_{-\infty}^{\infty} dE f(E + \epsilon_L^j) [1 - f(E)] = \epsilon_L^j n_B(\epsilon_L^j). \quad (\text{A32})$$

For the case of transverse spin-relaxation time, we take $\theta = \pi/2$, $\phi = \pi$. We have spin-flip operators $S_{-+}^{j,\perp} = S_j^z - iS_j^y$ and $S_{-+}^{j,\perp} = S_j^z + iS_j^y$. Then, the spin-spin correlation function becomes

$$D_{-+}^{j,\perp}(\omega) = +\frac{1}{4} [D_{-+}^{j,\parallel}(\omega) + D_{-+}^{j,\parallel}(\omega)] + \delta(\omega) \langle S_j^{\parallel} S_j^{\parallel} \rangle. \quad (\text{A33})$$

Then we obtain transverse spin-relaxation time

$$\frac{1}{\tau_{\perp}} = \frac{1}{2\tau_{\parallel}} + \frac{1}{\tau_{\phi}}, \quad (\text{A34})$$

with

$$\frac{1}{\tau_{\phi}} = \frac{\pi}{8\hbar} \sum_j n_j v_F (K_j^s)^2 \langle S_j^{\parallel} S_j^{\parallel} \rangle. \quad (\text{A35})$$

Here we have used the identities

$$D_{-+}^{j,\parallel}(\omega) = 2n_B(\epsilon_L^j) |\langle S_j^{\parallel} \rangle| \delta(\omega + \epsilon_L^j/\hbar), \quad (\text{A36})$$

$$\int_{-\infty}^{\infty} dE f(E - \epsilon_L^j) [1 - f(E)] = \epsilon_L^j [1 + n_B(\epsilon_L^j)]. \quad (\text{A37})$$

APPENDIX B: DIFFUSION EQUATION

In this section, we calculate the nonlocal resistance in Eq. (14) of the main text. Away from the boundaries, the diffusion equation can be written as follows:

$$\nabla^2 N^{\mu} - \mathcal{M}_v^{\mu} N^{\nu} = 0, \quad (\text{B1})$$

with

$$\mathcal{M}_v^{\mu} = \frac{1}{1 - \eta_s^2} \begin{bmatrix} \ell_v^{-2} & -\eta_s \ell_{sv}^{-2} \\ -\eta_s \ell_v^{-2} & \ell_{sv}^{-2} \end{bmatrix} \begin{matrix} v \\ sv \end{matrix}. \quad (\text{B2})$$

where η_s is the charge-to-spin conversion efficiency [Eq. (11)]. Only spin and valley densities are considered in the above equations because they are the only responses in the transverse direction to the applied electric field. In this expression, $\ell_v = \sqrt{D\tau^v}$ ($\ell_{sv} = \sqrt{D\tau^{sv}}$) is valley (spin-valley) diffusion length, where D is the diffusion coefficient. Here the valley relaxation time comes from valley-flip scattering induced by short-range disorders [37]. While the spin-valley relaxation time originates from the spin-valley-flip scattering

$$\frac{1}{\tau^{sv}} = \frac{1}{\tau_0} - \frac{\pi}{4\hbar} \sum_j n_j v_F (K_j^s)^2 \beta \epsilon_L^j n_B(\epsilon_L^j) [1 + n_B(\epsilon_L^j)] \langle S_j^{\parallel} \rangle. \quad (\text{B3})$$

Note that both spin- and valley-flip procedures result in the spin-valley flip. The spin-flip contribution has been expressed by the microscopic parameters, and spin expectations of the local moments within Weiss-field theory. Here, τ_0^{sv} is the external spin-valley relaxation time induced by such as intrinsic spin (valley)-orbit coupling or extrinsic spin (valley)-flip disorders, which is assumed to be independent of field and temperature. Note that the off-diagonal terms proportional to η_s mix the spin and spin-valley densities. Equation (B1) is solved by first finding the eigenvalues and eigenvectors of the diffusion matrix, i.e., $\mathcal{M}_v^{\mu} |\hat{\rho}_a^{\nu}\rangle = \mathcal{L}_a^{-2} |\hat{\rho}_a^{\nu}\rangle$, where \mathcal{L}_a ($a = 1, 2$) corresponds to the diffusion length of the eigenvector $|\hat{\rho}_a^{\nu}\rangle$.

Next, we solve the diffusion equation for a Hall bar device geometry, consisting of a channel of width W , which we assume to be infinitely long. We assume complete screening of the electric field in the device, which amounts to take charge density into zero, i.e., $N^c(\mathbf{r}) = 0$. Thus, we get Laplace equation $\nabla_r^2 \Phi(\mathbf{r}) = 0$. If we define nonlocal resistance as

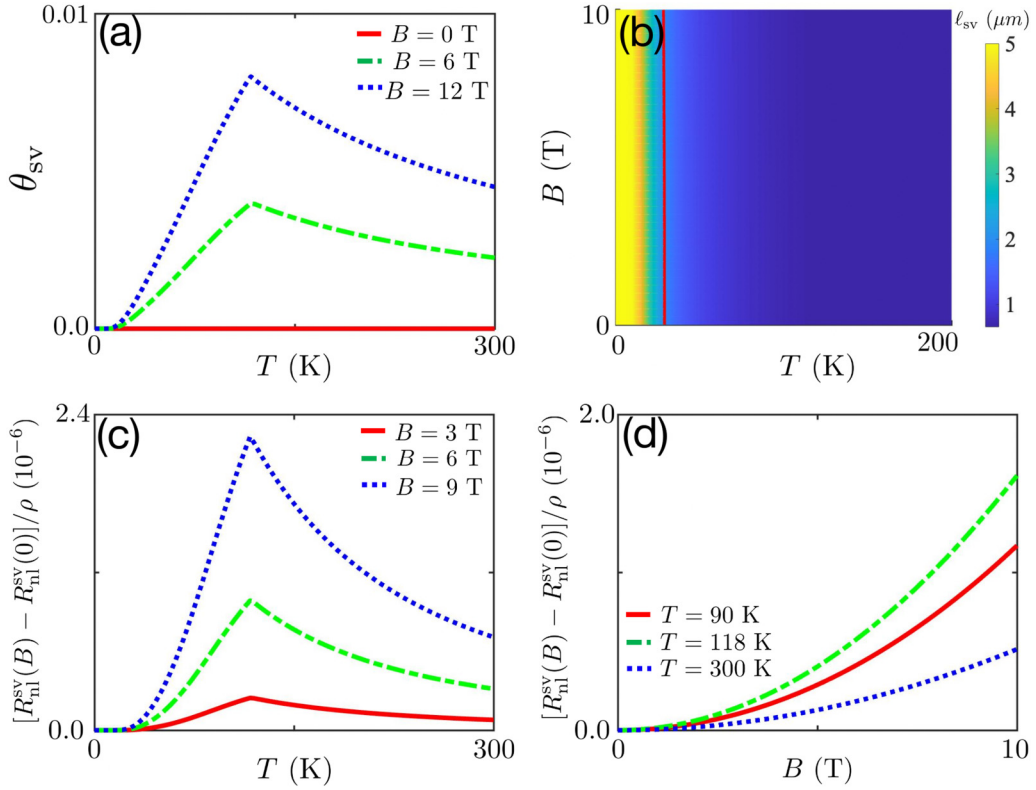


FIG. 4. The out-of-plane field and temperature dependence of SVHE for MnO substrate with Neel temperature $T_N = 118$ [80,81]. (a) Spin-valley Hall angle θ_{sv} as a function of temperature T (K) [Eq. (13)]. (b) Spin-valley diffusion length ℓ_{sv} as a function of temperature T and field B . The red line corresponds to $\ell_{sv} = X$ and the color bar is in the unit of μm . (c), (d) Relative nonlocal resistance of antiferromagnetic substrate, $[R_{nl}(B) - R_{nl}(0)]/\rho$, as a function of (c) temperature T and (d) magnetic field B . Parameters: $\ell_{sv}^{\text{max}} = 5\mu\text{m}$, $\ell_{sv}^{\text{min}} = 1\mu\text{m}$, $X = 2\mu\text{m}$, $W = 1\mu\text{m}$, and $K^s/K^o = 0.05$.

$R_{nl}(X) = (1/I)[\Phi(X, -W/2) - \Phi(X, +W/2)]$. Using the appropriate boundary conditions [37,82], we reach nonlocal resistance

$$R_{nl}(X) \simeq \underbrace{\rho \frac{4}{\pi} e^{-|X|/\mathcal{L}_o}}_{R_{nl}^o} + \sum_v \underbrace{\rho \frac{\theta_v^2}{1 + \theta_v^2} \frac{W}{2\mathcal{L}_v}}_{R_{nl}^v} e^{-|X|/\mathcal{L}_v}, \quad (\text{B4})$$

with $\mathcal{L}_v = \ell_v/(1 + \theta_v^2)^{1/2}$, where the first term is ohmic contribution, R_{nl}^o , and the second term is described by the summary of exponential dependence of each eigenmode, R_{nl}^v . Near the current injection point ($|X| \lesssim \ell_0$), R_{nl} is dominated by ohmic contribution, which will disappear at long enough distance ($|X| \gg \ell_0$). We focus on the behavior of R_{nl} . In the case of $\omega_v\tau \simeq 1$ and $\omega_s\tau \ll 1$, we obtain $\theta_v \simeq \omega_v\tau$, $\theta_{sv} \simeq \omega_s\tau$, and $\eta_s \simeq 0$. Thus, valley and spin-valley densities, are decoupled and can independently propagate along the Hall bar, as shown by Eq. (B2). The nonlocal resistance induced by the SVHE becomes

$$R_{nl}^{sv}(B, T) \simeq \theta_{sv}^2 \frac{W}{2\ell_{sv}} \rho e^{-|X|/\ell_{sv}}. \quad (\text{B5})$$

APPENDIX C: NONLOCAL RESISTANCE IN ANTIFERROMAGNET

In this section, we show the field and temperature dependence of SVHE in an antiferromagnetic insulator. Let us study the antiferromagnetic substrate, MnO. It has a typical Neel temperature $T_N = 118$ K [80,81]. The spins of two sublattices align antiparallel and cancel with each other in the absence of magnetic field. Hence, the magnetization of the antiferromagnetic insulator is much weaker. The temperature dependence of nonlocal resistance becomes much more interesting, especially for a temperature around Neel temperature, where the temperature dependence of magnetization (or spin-valley Hall angle) is not monotonic anymore, as shown in Fig. 4(a). This leads to similar behavior of nonlocal resistance [Fig. 4(c)]. Besides, we find maximal modulation of nonlocal resistance with the magnetic field at Neel temperature $T_N = 118$ K [green line of Fig. 4(d)]. Furthermore, it is hard to observe the negative nonlocal magnetoresistance effect [Fig. 4(d)], because of the weak modulation of spin-valley diffusion length with magnetic field [Fig. 4(b)].

[1] P. Wei, S. Lee, F. Lemaitre, L. Pinel, D. Cutaia, W. Cha, F. Katmis, Y. Zhu, D. Heiman, J. Hone *et al.*, *Nature Mater.* **15**, 711 (2016).

[2] C. Zhao, T. Norden, P. Zhang, P. Zhao, Y. Cheng, F. Sun, J. P. Parry, P. Taheri, J. Wang, Y. Yang *et al.*, *Nature Nanotechnol.* **12**, 757 (2017).

- [3] C. Tang, Z. Zhang, S. Lai, Q. Tan, and W.-b. Gao, *Adv. Mater.* **32**, 1908498 (2020).
- [4] C.-C. Tseng, T. Song, Q. Jiang, Z. Lin, C. Wang, J. Suh, K. Watanabe, T. Taniguchi, M. A. McGuire, D. Xiao *et al.*, [arXiv:2206.06949](https://arxiv.org/abs/2206.06949).
- [5] A. Kaverzin, T. S. Ghiasi, A. H. Dismukes, X. Roy, and B. J. van Wees, *2D Mater.* **9**, 045003 (2022).
- [6] T. S. Ghiasi, A. A. Kaverzin, A. H. Dismukes, D. K. de Wal, X. Roy, and B. J. van Wees, *Nature Nanotechnol.* **16**, 788 (2021).
- [7] A. G. Swartz, P. M. Odenthal, Y. Hao, R. S. Ruoff, and R. K. Kawakami, *ACS Nano* **6**, 10063 (2012).
- [8] T. Norden, C. Zhao, P. Zhang, R. Sabirianov, A. Petrou, and H. Zeng, *Nature Commun.* **10**, 4163 (2019).
- [9] B. Scharf, G. Xu, A. Matos-Abiague, and I. Žutić, *Phys. Rev. Lett.* **119**, 127403 (2017).
- [10] H.-X. Yang, A. Hallal, D. Terrade, X. Waintal, S. Roche, and M. Chshiev, *Phys. Rev. Lett.* **110**, 046603 (2013).
- [11] Y. Semenov, K. Kim, and J. Zavada, *Appl. Phys. Lett.* **91**, 153105 (2007).
- [12] D. Abanin, S. Morozov, L. Ponomarenko, R. Gorbachev, A. Mayorov, M. Katsnelson, K. Watanabe, T. Taniguchi, K. Novoselov, L. Levitov *et al.*, *Science* **332**, 328 (2011).
- [13] D. A. Abanin, R. V. Gorbachev, K. S. Novoselov, A. K. Geim, and L. S. Levitov, *Phys. Rev. Lett.* **107**, 096601 (2011).
- [14] H. Haugen, D. Huertas-Hernando, and A. Brataas, *Phys. Rev. B* **77**, 115406 (2008).
- [15] T. Zhou, J. Zhang, H. Jiang, I. Žutić, and Z. Yang, *npj Quantum Mater.* **3**, 39 (2018).
- [16] R. Gorbachev, J. Song, G. Yu, A. Kretinin, F. Withers, Y. Cao, A. Mishchenko, I. Grigorieva, K. S. Novoselov, L. Levitov *et al.*, *Science* **346**, 448 (2014).
- [17] W. Yao, D. Xiao, and Q. Niu, *Phys. Rev. B* **77**, 235406 (2008).
- [18] D. Xiao, W. Yao, and Q. Niu, *Phys. Rev. Lett.* **99**, 236809 (2007).
- [19] M. Ezawa, *Phys. Rev. B* **87**, 155415 (2013).
- [20] X. Li, T. Cao, Q. Niu, J. Shi, and J. Feng, *Proc. Natl. Acad. Sci. USA* **110**, 3738 (2013).
- [21] D. Xiao, G.-B. Liu, W. Feng, X. Xu, and W. Yao, *Phys. Rev. Lett.* **108**, 196802 (2012).
- [22] X.-P. Zhang, C. Huang, and M. A. Cazalilla, *Phys. Rev. B* **99**, 245106 (2019).
- [23] T. Zhou, S. Cheng, M. Schleenvoigt, P. Schüffelgen, H. Jiang, Z. Yang, and I. Žutić, *Phys. Rev. Lett.* **127**, 116402 (2021).
- [24] D. Wang, Z. Huang, Y. Zhang, and G. Jin, *Phys. Rev. B* **93**, 195425 (2016).
- [25] B. Soodchomshom, *J. Appl. Phys.* **115**, 023706 (2014).
- [26] M. M. Grujić, M. Ž. Tadić, and F. M. Peeters, *Phys. Rev. Lett.* **113**, 046601 (2014).
- [27] L. L. Tao and E. Y. Tsymbal, *Phys. Rev. B* **100**, 161110(R) (2019).
- [28] X.-J. Qiu, Z.-Z. Cao, J. Hou, and C.-Y. Yang, *Appl. Phys. Lett.* **117**, 102401 (2020).
- [29] M. Ezawa, *J. Phys. Soc. Jpn.* **84**, 121003 (2015).
- [30] S. F. Islam and C. Benjamin, *Carbon* **110**, 304 (2016).
- [31] M. Yarmohammadi, *J. Magn. Magn. Mater.* **426**, 621 (2017).
- [32] H. Yang, J. Xu, Z. Xiong, X. Lu, R.-Y. Zhang, H. Li, Y. Chen, and S. Zhang, *Phys. Rev. Lett.* **127**, 043904 (2021).
- [33] Z. Liu, W. Feng, H. Xin, Y. Gao, P. Liu, Y. Yao, H. Weng, and J. Zhao, *Mater. Horiz.* **6**, 781 (2019).
- [34] W.-T. Lu, Q.-F. Sun, Y.-F. Li, and H.-Y. Tian, *Phys. Rev. B* **104**, 195419 (2021).
- [35] A. L. Rakhmanov, A. V. Rozhkov, A. O. Sboychakov, and F. Nori, *Phys. Rev. Lett.* **109**, 206801 (2012).
- [36] I. L. Aleiner, D. E. Kharzeev, and A. M. Tsvelik, *Phys. Rev. B* **76**, 195415 (2007).
- [37] X.-P. Zhang, C. Huang, and M. A. Cazalilla, *2D Mater.* **4**, 024007 (2017).
- [38] F. Guinea, M. Katsnelson, and A. Geim, *Nature Phys.* **6**, 30 (2010).
- [39] M. A. Vozmediano, M. Katsnelson, and F. Guinea, *Phys. Rep.* **496**, 109 (2010).
- [40] M. I. Katsnelson, *Graphene: Carbon in Two Dimensions* (Cambridge University Press, Cambridge, 2012)
- [41] B. Amorim, A. Cortijo, F. De Juan, A. Grushin, F. Guinea, A. Gutiérrez-Rubio, H. Ochoa, V. Parente, R. Roldán, P. San-Jose *et al.*, *Phys. Rep.* **617**, 1 (2016).
- [42] M. A. Ruderman and C. Kittel, *Phys. Rev.* **96**, 99 (1954).
- [43] L. Fritz and M. Vojta, *Rep. Prog. Phys.* **76**, 032501 (2013).
- [44] S. Lara-Avila, S. Kubatkin, O. Kashuba, J. A. Folk, S. Lüscher, R. Yakimova, T. J. B. M. Janssen, A. Tzalenchuk, and V. Fal'ko, *Phys. Rev. Lett.* **115**, 106602 (2015).
- [45] X.-P. Zhang, F. S. Bergeret, and V. N. Golovach, *Nano Lett.* **19**, 6330 (2019).
- [46] C. P. Slichter, *Principles of Magnetic Resonance*, (Springer Science & Business Media, Berlin, 2013) Vol. 1.
- [47] J. Balakrishnan, G. K. W. Koon, A. Avsar, Y. Ho, J. H. Lee, M. Jaiswal, S.-J. Baeck, J.-H. Ahn, A. Ferreira, M. A. Cazalilla, and A. H. Castro Neto, *Nature Commun.* **5**, 4748 (2014).
- [48] J. Balakrishnan, G. K. W. Koon, M. Jaiswal, A. H. C. Neto, and B. Özyilmaz, *Nature Phys.* **9**, 284 (2013).
- [49] A. A. Kaverzin and B. J. van Wees, *Phys. Rev. B* **91**, 165412 (2015).
- [50] A. Avsar, J. H. Lee, G. K. W. Koon, and B. Özyilmaz, *2D Mater.* **2**, 044009 (2015).
- [51] Y. Wang, X. Cai, J. Reutt-Robey, and M. S. Fuhrer, *Phys. Rev. B* **92**, 161411(R) (2015).
- [52] C. Huang, Y. D. Chong, and M. A. Cazalilla, *Phys. Rev. B* **94**, 085414 (2016).
- [53] C. Huang, Y. D. Chong, and M. A. Cazalilla, *Phys. Rev. Lett.* **119**, 136804 (2017).
- [54] A. A. Burkov, A. S. Núñez, and A. H. MacDonald, *Phys. Rev. B* **70**, 155308 (2004).
- [55] A. A. Burkov and D. G. Hawthorn, *Phys. Rev. Lett.* **105**, 066802 (2010).
- [56] N. Levy, S. Burke, K. Meaker, M. Panlasigui, A. Zettl, F. Guinea, A. C. Neto, and M. F. Crommie, *Science* **329**, 544 (2010).
- [57] C. Huang, Y. D. Chong, G. Vignale, and M. A. Cazalilla, *Phys. Rev. B* **93**, 165429 (2016).
- [58] K. F. Mak, K. L. McGill, J. Park, and P. L. McEuen, *Science* **344**, 1489 (2014).
- [59] S.-Q. Shen, *Phys. Rev. Lett.* **95**, 187203 (2005).
- [60] B. Zhou, L. Ren, and S.-Q. Shen, *Phys. Rev. B* **73**, 165303 (2006).
- [61] W. Müller and W. Nolting, *Phys. Rev. B* **66**, 085205 (2002).
- [62] J. Sinova, S. O. Valenzuela, J. Wunderlich, C. H. Back, and T. Jungwirth, *Rev. Mod. Phys.* **87**, 1213 (2015).

- [63] K. Oyanagi, J. M. Gomez-Perez, X.-P. Zhang, T. Kikkawa, Y. Chen, E. Sagasta, A. Chuvilin, L. E. Hueso, V. N. Golovach, F. S. Bergeret *et al.*, *Phys. Rev. B* **104**, 134428 (2021).
- [64] J. M. Gomez-Perez, X.-P. Zhang, F. Calavalle, M. Ilyn, C. González-Orellana, M. Gobbi, C. Rogero, A. Chuvilin, V. N. Golovach, L. E. Hueso *et al.*, *Nano Lett.* **20**, 6815 (2020).
- [65] J. S. Moodera, T. S. Santos, and T. Nagahama, *J. Phys.: Condens. Matter* **19**, 165202 (2007).
- [66] J. H. van Vleck, *Phys. Rev.* **52**, 1178 (1937).
- [67] J. G. Gay and R. Richter, *Phys. Rev. Lett.* **56**, 2728 (1986).
- [68] A. W. Cummings, J. H. Garcia, J. Fabian, and S. Roche, *Phys. Rev. Lett.* **119**, 206601 (2017).
- [69] L. A. Benítez, J. F. Sierra, W. S. Torres, A. Arrighi, F. Bonell, M. V. Costache, and S. O. Valenzuela, *Nature Phys.* **14**, 303 (2018).
- [70] T. S. Ghiasi, J. Ingla-Aynés, A. A. Kaverzin, and B. J. van Wees, *Nano Lett.* **17**, 7528 (2017).
- [71] M. Gmitra and J. Fabian, *Phys. Rev. B* **92**, 155403 (2015).
- [72] M. Gmitra, D. Kochan, P. Högl, and J. Fabian, *Phys. Rev. B* **93**, 155104 (2016).
- [73] D. A. Abanin, A. V. Shytov, L. S. Levitov, and B. I. Halperin, *Phys. Rev. B* **79**, 035304 (2009).
- [74] T. Jungwirth, J. Sinova, J. Mašek, J. Kučera, and A. H. MacDonald, *Rev. Mod. Phys.* **78**, 809 (2006).
- [75] V. G. Storchak, D. G. Eshchenko, E. Morenzoni, T. Prokscha, A. Suter, X. Liu, and J. K. Furdyna, *Phys. Rev. Lett.* **101**, 027202 (2008).
- [76] I. Žutić, J. Fabian, and S. Das Sarma, *Phys. Rev. Lett.* **88**, 066603 (2002).
- [77] C. Weeks, J. Hu, J. Alicea, M. Franz, and R. Wu, *Phys. Rev. X* **1**, 021001 (2011).
- [78] I. Žutić, J. Fabian, and S. D. Sarma, *Rev. Mod. Phys.* **76**, 323 (2004).
- [79] B. E. Kane, *Nature (London)* **393**, 133 (1998).
- [80] C. Rao and G. Subba Rao, *Phys. Stat. Sol. (a)* **1**, 597 (1970).
- [81] M. S. Jagadeesh and M. S. Seehra, *Phys. Rev. B* **23**, 1185 (1981).
- [82] M. Beconcini, F. Taddei, and M. Polini, *Phys. Rev. B* **94**, 121408(R) (2016).